Fiber-optic Fourier-domain common-path OCT

Xuan Liu[1], Xiaolu Li[1], Do-Hyun Kim[2], Ilko Ilev[2], and Jin U. Kang[1]

[1]*Department of Electrical and Computer Engineering, Johns Hopkins University, 3400 N. Charles Street, Baltimore, MD, 21218, USA*

[2]*Center for Devices and Radiological Health, FDA, 10903 New Hampshire Avenue, Silver Spring, MD 20993-0002, USA*

Received August 27, 2008

We experimentally and theoretically investigated the performance of a fiber-optic based Fourier-domain common-path optical coherence tomography (OCT). The fiber-optic common-path OCT operated at the 840-nm center wavelength. The resolution of the system was 8.8 μm (in air) and the working depth using a bare fiber probe was approximately 1.5 mm. The signal-to-noise ratio (SNR) of the system was analyzed. OCT images obtained by the system were also presented.

OCIS codes: 110.4500, 070.0070.

doi: 10.3788/COL20080612.0899.

Low-coherence interferometer is the core of any optical coherence tomography (OCT) systems. Therefore, the design of interferometer is an important step that would determine the system performance[1]. In common-path OCT (CP-OCT), a common-path interferometer set-up is used, in which the sample and reference lights share the same path[2]. With fiber optical devices, one can build a robust and compact CP-OCT system. The probe arm in CP-OCT can have arbitrary length, which is favorable for endoscopic applications[3,4]. Besides, the shared probe arm helps to circumvent the problem of chromatic dispersion, which is not neglectable in high-resolution OCT systems that use separate sample and reference arms. Hence CP-OCT system can potentially be used in obtaining high and ultra high resolution OCT images. It is known that Fourier-domain OCT (FD-OCT) can have higher imaging speed than time domain OCT (TD-OCT), and has better signal-to-noise ratio (SNR) performance[5,6]. Thus, Fourier-domain common-path OCT (FD-CP-OCT) that combines the advantages of CP- and FD-OCT can potentially be highly beneficial[7−9]. In this letter, we present our work on FD-CP-OCT. The SNR of the system is studied. We achieve an axial resolution of 8.8 μm (in air). Images of different samples are also presented.

Figure 1 shows the schematic of the FD-CP-OCT system. The broadband light from a super luminescence light emitting diode (SLED) operating at 840 nm is split by a 50/50 fiber coupler. An optical fiber with its tip cleaved in right angle is used as a probe. The glass-air interface at the end of fiber probe reflects the light back and provides the reference light. The light from the inside of the sample and the reference surface combines together and is analyzed by a custom configured high resolution fiber optic spectrometer (HR 4000, Ocean Optics Inc.). The spectrometer covers a spectral range from 700 to 900 nm and uses a charge-coupled device (CCD) array with 3648 pixels. The maximum imaging depth of the system is approximately 3.5 mm, corresponding to the spectral resolution of 0.09 nm. However, the penetrating depth of our system is smaller than 3.5 mm, because the illumination beam is diverging. The beam radius gets larger when propagating in the sample, which causes signal to decrease. Another factor that limits the working depth is multiple scattering. Our measured working distance is about 1.5 mm. The data from the spectrometer is converted from the wavelength space to the wavevector space and fast Fourier transform (FFT) is performed to reconstruct the longitudinal profile of samples. Lateral scan is performed by a Galvanometer which sweeps the bare fiber probe in front of the sample. The scanning control, data acquisition, processing, and image display are implemented using a homemade Labview program.

The FD-OCT signal amplitude can be written as[5]

$$S_{\text{peak}} = \frac{S\eta\tau}{Nh\nu_0}\sqrt{P_{\text{r}}P_{\text{s}}}, \tag{1}$$

which is a dimensionless quantity. Here, S is the spectrometer efficiency, η is detector quantum efficiency, τ is the CCD exposure time, N is the number of CCD pixels, h is the Planck constant, v_0 is the center frequency of the light source spectrum, P_{s} is the sample power, and P_{r} is the reference power.

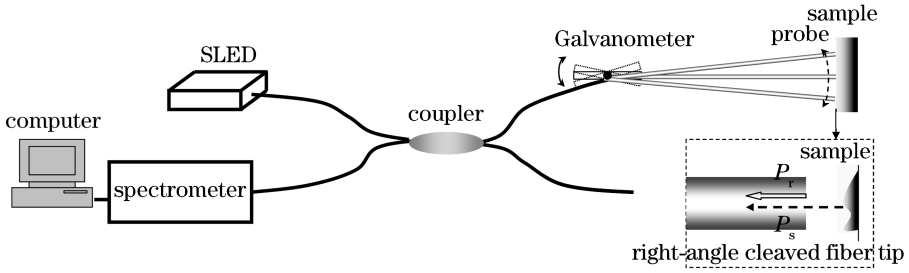

Fig. 1. Schematic diagram of the FD-CP-OCT system. A bare fiber probe is used as a probe, as shown in the dashed box.

The main noise sources in FD-OCT systems are receiver noise, shot noise, and excess noise[3]. The receiver noise includes dark noise $\sigma^2_{\rm dark}$ and read noise $\sigma^2_{\rm read}$. In our system, the dark noise is about 8 counts and the read noise is about 50 counts.

The excess noise of the FD-CP-OCT is given by

$$\sigma^2_{\rm excess} = \frac{1+V^2}{2\delta v'}\left(\frac{S\eta}{h\nu_0}\frac{P_{\rm r}+P_{\rm s}}{N}\right)^2\tau, \tag{2}$$

where V is the degree of polarization and $\delta v' = \Delta v_{\rm eff}/N$. $\Delta v_{\rm eff}$ is the effective spectral line width[1].

The shot noise is given by

$$\sigma^2_{\rm shot} = \frac{S\eta\tau}{h\nu_0}\frac{P_{\rm r}+P_{\rm s}}{N}. \tag{3}$$

If we assume the noise originated from different CCD pixels is additive, independent, and white, they will combine incoherently after FFT. In other words, they add in intensity instead of amplitude. The total noise after FFT is then given by

$$\sigma^2_{\rm noise} = \left(\sigma^2_{\rm shot}+\sigma^2_{\rm excess}+\sigma^2_{\rm dark}+\sigma^2_{\rm read}\right)\frac{1}{N}. \tag{4}$$

The SNR can be written as

$$\mathrm{SNR} = 10\lg\left(\frac{S^2_{\rm peak}}{\sigma^2_{\rm noise}}\right). \tag{5}$$

A mirror is used as a sample for analyzing the SNR of the system. Only does a small fraction of light reflected by the mirror couple back to the probe. To study the SNR of the FD-CP-OCT system, we changed the source power, while keeping the mirror and the fiber probe fixed. We measured the SNR as a function of the reference power which is plotted in Fig. 2 based on Eq. (5) and recorded the spectra under different power output. Using the measured spectra, we calculated the A-scan signal and SNR, as shown in Fig. 2. From Fig. 2, it is clear that there is a large difference of 10 to 15 dB between the theoretical expected SNR and the actual experimental value.

The amplitude of the A-scan signal peak can be written in the following way:

$$S_{\rm peak} = \frac{1}{N}\sqrt{\left(\frac{S\eta\tau}{h\nu_0}P_{\rm r}\right)\left(\frac{S\eta\tau}{h\nu_0}P_{\rm s}\right)} = \frac{1}{N}\sqrt{N_{\rm pr}N_{\rm ps}}. \tag{6}$$

The counts at each pixel are proportional to the optical energy incident onto that pixel. The summation of counts of all the pixels is proportional to the optical energy incident onto the spectrometer. $N_{\rm pr}$ and $N_{\rm ps}$ are summations of counts corresponding to the reference power and the sample power, respectively. We can readily get $N_{\rm pr}$ and $N_{\rm ps}$ from our spectral measurements, and thus $S_{\rm peak}$. However, the actual peak amplitude $\widehat{S}_{\rm peak}$ of A-scan obtained by Fourier transforming the interferogram is much smaller than the expected $S_{\rm peak}$. There are several reasons for such difference. Firstly, the experimental axial resolution is worse than the theoretical one, which means that the amplitude is diminished while the impulse response is broadened. Secondly, the interferometer is not an ideally sinusoidal signal modulator, the random phase noise occur over the extra signal pass makes $\widehat{S}_{\rm peak}$ smaller. In addition, the nonlinear and nonuniform response of the detector array appear as a phase noise and reduces the SNR.

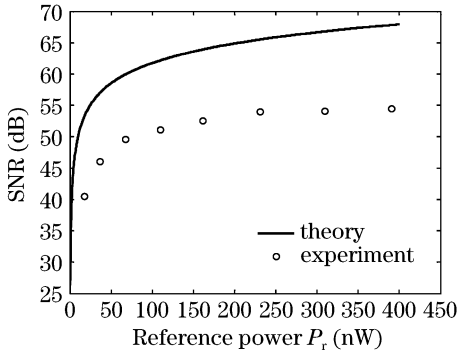

Fig. 2. Theoretical and experimental SNR as a function of reference power.

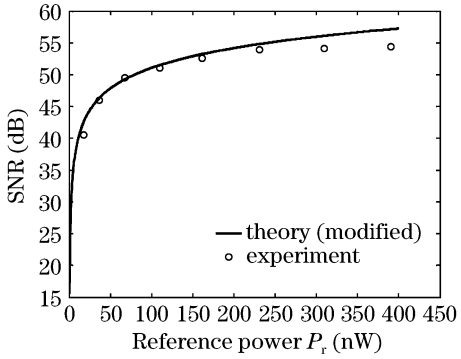

Fig. 3. Modified theoretical and experimental SNR as a function of reference power.

After we take this empirical ratio $r = \widehat{S}_{\rm peak}/S_{\rm peak}$ into consideration, the modified SNR shown in Eq. (6) can be written as

$$\mathrm{SNR} = 10\lg\left(r^2\frac{S^2_{\rm peak}}{\sigma^2_{\rm noise}}\right). \tag{7}$$

It is noted that the modified theoretical SNR and experimental SNR match well in Fig. 3. This result shows that our noise model is reasonable, but we overestimated the signal amplitude when computing theoretical SNR curve in Fig. 2.

The source (SLED, EXS8410-2413) was centered at 840 nm with full-width at half-maximum (FWHM) of 40 nm, corresponding to theoretical axial resolution of 7.8 μm. However, the actual resolution of the system was approximately 8.8 μm which was obtained experimentally using a mirror as a sample. The maximum source output from the probe end was 0.5 mW. Figure 4 shows the images obtained by the FD-CP-OCT system. Figure 4(a) is an image of multiple layers of 80-μm thick cellophane film with thin layers of epoxy in between which are clearly visible. Figure 4(b) is an image of a sardine spine, and Fig. 4(c) is an image of a part of a cricket head.

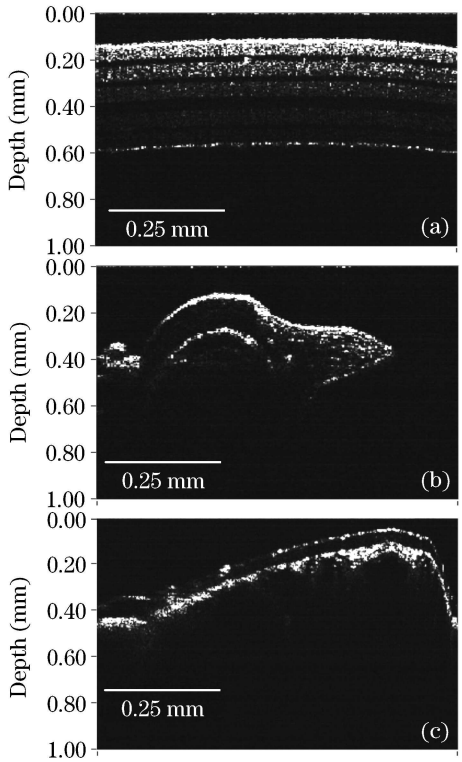

Fig. 4. OCT images of (a) cellophane films, (b) a sardine spine, and (c) a cricket head.

In conclusion, we built and investigated a FD-CP-OCT with a depth resolution of 8.8 μm. The SNR of the system was studied and discussed. We took the empirical ratio into consideration in order to modify SNR of our FD-CP-OCT system. It has shown that the modified theoretical SNR and experimental SNR match well with each other and our new SNR model is reasonable. From this work, it is clear that the ideal theoretical SNR is significantly higher than the experimental one because we assumed ideal response from all the fiber components and the detector array. From the result of the experiment, when the detected reference power is larger than 200 nW, we can achieve SNR as high as 55 dB.

X. Liu's e-mail address is xliu35@jhu.edu.

References

1. A. M. Rollins and J. A. Izatt, Opt. Lett. **24,** 1484 (1999).
2. U. Sharma, N. M. Fried, and J. U. Kang, IEEE J. Sel. Top. Quantum Electron. **11,** 799 (2005).
3. Y. Yang, Z. Ding, J. Meng, L. Wu, Z. He, T. Wu, and M. Chen, Proc. SPIE **6826,** 1S1 (2007).
4. A. R. Tumlinson, J. K. Barton, B. Považay, H. Sattman, A. Unterhuber, R. A. Leitgeb, and W. Drexler, Opt. Express **14,** 1878 (2006).
5. R. Leitgeb, C. K. Hitzenberger, and A. F. Fercher, Opt. Express **11,** 889 (2003).
6. S. H. Yun, G. J. Tearney, B. E. Bouma, B. H. Park, and J. F. de Boer, Opt. Express **11,** 3598 (2003).
7. A. Popp, M. Wendel, L. Knels, P. Knuschke, M. Mehner, T. Koch, and E. Koch, Proc. SPIE **5861,** 58610Q-1 (2005).
8. A. B. Vakhtin, D. J. Kane, W. R. Wood, and K. A. Peterson, Appl. Opt. **42,** 6953 (2003).
9. J. U. Kang and A. Rodriguez, *CLEO 2007,* JTuA55 (2007).